

Electron Tunneling Spectroscopy of the anisotropic Kitaev Quantum Spin Liquid Sandwiched with Superconductors

Shi-Qing Jia and Liang-Jian Zou*

Key Laboratory of Materials Physics, Institute of Solid State Physics,
HFIPS, Chinese Academy of Sciences, Hefei 230031, China and

Science Island Branch of Graduate School, University of Science and Technology of China, Hefei 230026, China

Ya-Min Quan

Key Laboratory of Materials Physics, Institute of Solid State Physics,
HFIPS, Chinese Academy of Sciences, Hefei 230031, China

Hai-Qing Lin†

Beijing Computational Science Research Center, Beijing 100193, China and
Department of Physics, Beijing Normal University, Beijing 100875, China

(Dated: March 10, 2022)

We present the electron tunneling transport and spectroscopic characters of a superconducting *Josephson* junction with a barrier of single anisotropic Kitaev quantum spin liquid (QSL) layer. We find that the dynamical spin correlation features are well reflected in the direct-current differential conductance dI^c/dV of the single-particle tunneling, including the unique spin gap and dressed itinerant Majorana dispersive band, in addition to an energy shift 2Δ of two-lead superconducting gaps. From the spectral characters, we identify different topological quantum phases of the anisotropic Kitaev QSL. We also present the zero-voltage *Josephson* current I^s which displays residual features of the anisotropic Kitaev QSL. These results pave a new way to measure the dynamical spinon or Majorana fermion spectroscopy of the Kitaev and other spin liquid materials.

PACS numbers: 75.10.Kt, 75.10.Jm, 74.50.+r

I. INTRODUCTION

The quantum spin liquid (QSL) phase, which consists of various spin singlet pairings in the spin structure without breaking any constituent symmetries of their underlying lattice, has attracted great attention [1, 2]. Enormous efforts have been made to understand the essence of the QSLs, and earlier studies focused on the geometrically and magnetic frustrated interaction [3, 4]. However, the essence and unique characters of the QSL states remain great debates [5, 6]. More than a decade ago Kitaev proposed an exactly solvable model on the two-dimension (2D) honeycomb lattice [7], which shows that the interaction frustration drives a ground state of gapless or gapped Z_2 QSL with fractionalized excitations [8]. The QSL state with gapped excitations has the Abelian anyons [9], the one with gapless excitations may have the non-Abelian anyon excitations [10]. Due to topological protection and large degeneracy of these anyons, the Majorana fermion excitations and its braiding group in the gapless QSL state were expected to be applicable for the quantum computing storage and quantum computation [8, 11]. However, how to excite and detect the dynamics of these Majorana fermion modes in Kitaev systems remains unknown.

On the other hand, the *Josephson* tunneling junctions,

which are constructed of two superconducting (SC) leads separated by an insulating or metallic barrier, provide a well probe to measure the quasi-particle information of the central region through the quantum tunneling transport [12, 13]. A great deal of central materials, such as insulators [14], normal metals [15], quantum dots [16–18], ferromagnets [19–21] and antiferromagnets [22, 23] have been studied. In order to explore the exotic spin correlations and fractional excitations of the Majorana fermions through the transports of single electrons and Cooper pairs, especially the inelastic spin scattering process [24–26], it is worth constructing novel SC-Kitaev layer-SC tunneling junctions to reveal its current dynamics associated with exotic spin excitations in Kitaev layer. In realistic candidate materials for the Kitaev layer, the spin interactions are usually anisotropic [27–30], thus we employ anisotropic Kitaev layer in the designed SC *Josephson* junctions.

In this *paper*, we utilize the current and conductance features of the SC-anisotropic Kitaev layer-SC tunneling junctions to characterize the dynamical spin correlations of the central-zone Kitaev materials. We adopt the non-equilibrium Green's function [17] and the few-particle response method [31, 32] to obtain the formulae of the single-particle and *Josephson* tunneling currents. We find that the dynamical spin susceptibility explicitly displays in the direct current (DC) single-particle differential conductance spectrum dI^c/dV , and from its spectral features, we could confirm the different topological quantum phases of the anisotropic Kitaev QSL. One ex-

* zou@theory.issp.ac.cn

† haiqing0@csrc.ac.cn

pects that the SC-anisotropic Kitaev QSL-SC mesoscopic hybrid systems with weak links may open a fruitful research field, not only because of the abundant fundamental features from the interplay between Kitaev physics and SC, but also of the potential application for design and development of new quantum devices.

II. MODEL AND TUNNELING OF THE SC-KITAEV QSL-SC JUNCTION

A. The SC-Kitaev QSL-SC junction and tunneling process

We construct a Kitaev Josephson junction, where a single-layer Kitaev insulator is the barrier, sandwiched by two leads consisting of two conventional s-wave superconductors. Here the SC leads may be Nb, or Pb metals, or their alloys NbTi and Nb₃Sn, *etc.*, and the central Kitaev layer may be α -RuCl₃ or Na₂IrO₃ single layer, which are the candidate materials of the Kitaev QSL [29]. Such a SC-Kitaev QSL-SC *Josephson* junction is shown in Fig. 1. Since the Kitaev material is a kind of transition-metal Mott insulator with strong electronic correlation, the tunneling of conduction electrons between left and right SC leads is scattered by the local spins in the central region, as shown in Fig. 2. The scattering strength is $s - d$ -type exchange coupling J .

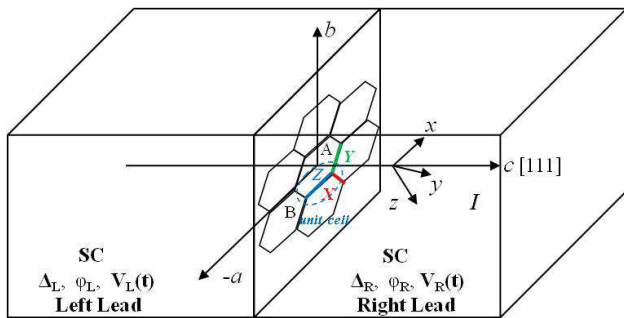


FIG. 1. (Color online) Schematic superconductor-Kitaev QSL-superconductor tunneling junction. The left (right) side is the SC lead with gap Δ_L (Δ_R), phase ϕ_L (ϕ_R) and electric potential $V_L(t)$ ($V_R(t)$). The central region is a single-layer Kitaev material in the ab plane.

For this set-up, the tunneling current consists of normal single-particle one and Josephson one. We can describe the normal single-particle tunneling process as follows: firstly, the electrons at the bottom of SC gap in the right lead enter the Kitaev layer, and occupy the high energy levels to form the virtual double occupied states. The propagation of the electrons would be modulated by the dynamical spin susceptibility of the Kitaev QSL in the spin-conserving channel, as well as in the spin-flipping process with spin fluctuations. Finally, the electrons leave the Kitaev layer with constant or opposite spins and go to the top of the SC gap in the left SC lead.

Moreover, the tunneling process of the SC Cooper pairs can be addressed as follows: the Cooper pair in the right lead firstly tunnels into the central Kitaev region, splitting as the quasi-electron and quasi-hole with opposite spins. Afterwards, the quasi-electron and quasi-hole would go through the similar virtual transitions as the single particles with the modulation of the Kitaev QSL. Once tunneling out of the central Kitaev region, the separated quasi-electrons and quasi-holes would recombine to SC Cooper pairs. These tunneling processes of single particles and Cooper pairs could be qualitatively described by the sketched diagram shown in Fig. 2.

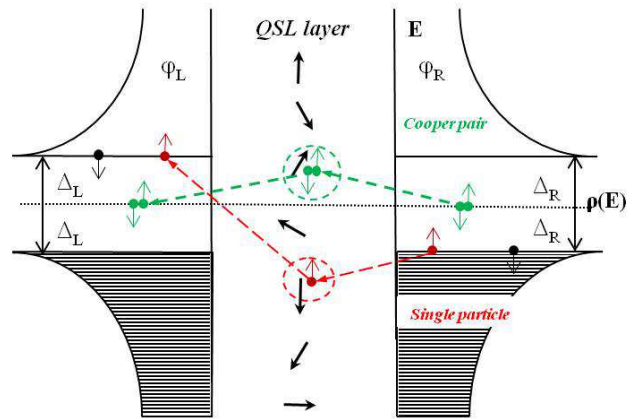


FIG. 2. (Color online) Sketched diagram of the single-particle (red) and Cooper pair (green) tunneling processes in the superconductor-Kitaev QSL-superconductor *Josephson* junction. The left and right sides are the bare density-of-states (DOS) distributions $\rho(E)$ of the two SC leads, and the center is the Kitaev QSL layer. The circles indicate the $s - d$ exchange processes of single particle and a Cooper pair with local spin, respectively.

B. Model Hamiltonian and Formulae

The total Hamiltonian of the SC-Kitaev QSL-SC tunneling junction shown in Fig. 1 and Fig. 2 consists of three parts as follows: the left and right SC electrodes $H_{Lead,n}$ ($n = L, R$), the single-layer Kitaev material in the central scattering region H_{cen} , and the $s - d$ exchange interaction part between the SC leads and central material H_T . So $H = \sum_{n=L,R} H_{Lead,n} + H_{cen} + H_T$, and

$$\begin{aligned}
 H_{Lead,n} &= \sum_{k\sigma} \epsilon_{nk\sigma}^0 a_{nk\sigma}^\dagger a_{nk\sigma} + \sum_k \Delta_n [a_{n,-k\downarrow} a_{nk\uparrow} + h.c.], \\
 H_{cen} &= -K_X \sum_{\langle ij \rangle_X} \hat{\sigma}_i^x \hat{\sigma}_j^x - K_Y \sum_{\langle ij \rangle_Y} \hat{\sigma}_i^y \hat{\sigma}_j^y - K_Z \sum_{\langle ij \rangle_Z} \hat{\sigma}_i^z \hat{\sigma}_j^z, \quad (1) \\
 H_T &= - \sum_i \left\{ \frac{1}{2} \tilde{J}_i(t) \left[\hat{\sigma}_i^z \left(a_{Li\uparrow}^\dagger a_{Ri\uparrow} - a_{Li\downarrow}^\dagger a_{Ri\downarrow} \right) \right. \right. \\
 &\quad \left. \left. + \hat{\sigma}_i^+ a_{Li\downarrow}^\dagger a_{Ri\uparrow} + \hat{\sigma}_i^- a_{Li\uparrow}^\dagger a_{Ri\downarrow} \right] + h.c. \right\},
 \end{aligned}$$

where $a_{nk\sigma}^\dagger$ and $c_{i\sigma}^\dagger$ are the creation operators of electrons in the SC leads and Kitaev layer, respectively, and $a_{ni\sigma}^\dagger$ is the Fourier transform of $a_{nk\sigma}^\dagger$ on the i th site of the 2D interface between the SC leads and Kitaev layer. $\hat{\sigma}_i^{x(y,z)} = \sum_{\sigma\sigma'} c_{i\sigma}^\dagger \sigma_{\sigma\sigma'}^{x(y,z)} c_{i\sigma'}$ are the twice spin components, $\hat{\sigma}_i^\pm = \hat{\sigma}_i^x \pm i\hat{\sigma}_i^y$, and $\sigma_{\sigma\sigma'}^{x(y,z)}$ are the Pauli matrices. Let the two SC leads be the s -wave superconductors and their order parameters $\tilde{\Delta}_n = \Delta_n e^{-i\phi_n}$ with magnitudes Δ_n and phases ϕ_n . $\epsilon_{nk\sigma}^0$ is the single-electron energy. K_X , K_Y and K_Z are the spin coupling constants along the X , Y and Z bonds in the central Kitaev layer, and they satisfy the conditions $K_X = K_Y > 0$ and $K_X + K_Y + K_Z = 3K$ for the anisotropic Kitaev model. J_i is the s - d exchange matrix element between the electrons in the SC leads and the local spins in Kitaev layer. In the presence of external electric potential $V_n(t)$ ($n = L, R$), the exchange parameter becomes voltage dependence of $\tilde{J}_i(t) = J_i \exp[i(\phi_L - \phi_R) - (i/\hbar) \int_0^t e(V_L(t_1) - V_R(t_1)) dt_1]$ through a unitary transformation, leaving only the perturbation term H_T explicitly depends on time [16].

The tunneling current from the left SC lead to the central region reads,

$$I(t) = -e \left\langle \frac{dN_L(t)}{dt} \right\rangle = \frac{ie}{\hbar} \langle [N_L(t), H(t)] \rangle \quad (2)$$

$$= -\frac{e}{\hbar} \text{Re} \sum_i \tilde{J}_i(t) i \left\langle \begin{array}{l} \hat{\sigma}_i^z (a_{Li\uparrow}^\dagger a_{Ri\uparrow} - a_{Li\downarrow}^\dagger a_{Ri\downarrow}) \\ + \hat{\sigma}_i^+ a_{Li\downarrow}^\dagger a_{Ri\uparrow} + \hat{\sigma}_i^- a_{Li\uparrow}^\dagger a_{Ri\downarrow} \end{array} \right\rangle.$$

It actually contains two parts: the normal single-particle tunneling current and SC *Josephson* current, and both of them stem from the inelastic scattering with the spin-conserving ($m = zz$) and spin-flipping ($m = xx, yy$) processes,

$$I(t) = -\frac{2e}{\hbar} \text{Re} \sum_{ij,m} \int_{-\infty}^t \frac{dt_1}{\hbar} J_i J_j \quad (3)$$

$$\left\{ \begin{array}{l} e^{\frac{ieV(t-t_1)}{\hbar}} \left[\begin{array}{l} \tilde{g}_{m,LR,ij}^r(t, t_1) G_{m,ji}^<(t_1, t) \\ + \tilde{g}_{m,LR,ij}^<(t, t_1) G_{m,ji}^a(t_1, t) \end{array} \right] \\ + e^{\frac{ieV(t+t_1)}{\hbar}} e^{i\phi} \left[\begin{array}{l} \tilde{g}_{m,LR,ij}^{r'}(t, t_1) G_{m,ji}^<(t_1, t) \\ + \tilde{g}_{m,LR,ij}^{<'}(t, t_1) G_{m,ji}^a(t_1, t) \end{array} \right] \end{array} \right\}.$$

Throughout this paper we only consider the DC voltage $V = V_L - V_R$ and $\phi = \phi_L - \phi_R$ is the phase difference between the left and right SC leads. Define $G(g)_{m,ji}^{r,a,<}$ with superscripts r , a , and $<$ as the dressed (bare) retarded, advanced, and lesser Green's functions of spin correlation in the central region, respectively. $\tilde{g}_{m,LR,ij}^{r,a,<}(t, t_1)$ and $\tilde{g}_{m,LR,ij}^{r',a,<}(t, t_1)$ are bare normal and anomalous Green's functions of electron-hole modes and Cooper pairs between left and right SC leads, respectively. For example, the advanced Green's functions can

be written as follows:

$$g_{m,ji}^r(t_1, t) = -i\theta(t_1 - t) \langle [0.5\hat{\sigma}_j^\alpha(t_1), 0.5\hat{\sigma}_i^\alpha(t)] \rangle, \quad (4)$$

$$\tilde{g}_{m,LR,ij}^r(t, t_1) = -i\theta(t - t_1) \langle [\hat{\sigma}_{\sigma\sigma'}^\alpha a_{Li\sigma}^\dagger a_{Ri\sigma'}(t), \hat{\sigma}_{\sigma\sigma'}^\alpha a_{Lj\sigma}^\dagger a_{Lj\sigma'}(t_1)] \rangle,$$

$$\tilde{g}_{m,LR,ij}^{r'}(t, t_1) = -i\theta(t - t_1) \langle [\hat{\sigma}_{\sigma\sigma'}^\alpha a_{Li\sigma}^\dagger a_{Ri\sigma'}(t), \hat{\sigma}_{\sigma\sigma'}^\alpha a_{Lj\sigma}^\dagger a_{Rj\sigma'}(t_1)] \rangle,$$

where $m = \alpha\alpha$, $\alpha = x, y, z$. The details are shown in Sec. A of *Supplementary Materials* [33].

With zero bias voltage, we have only DC *Josephson* current I^s generated by the tunneling of Cooper electron pairs through the Kitaev QSL. Moreover, at $V \neq 0$, we are much interested at the DC current I^c and its conductance dI^c/dV of the normal single-particle tunneling. Thus, the DC single-particle and *Josephson* current terms in the first-order approximation can be obtained as follows:

$$I^c = \frac{4e}{\hbar} \sum_{ij,m} \int \frac{d\epsilon}{2\pi} J_i J_j \text{Im} [\tilde{g}_{m,LR,ij}^r(eV - \epsilon)] \quad (5)$$

$$\text{Im} [g_{m,ij}^r(\epsilon)] [n(\epsilon) - n(\epsilon - eV)],$$

$$I^s = \frac{4e}{\hbar} \sum_{ij,m} \int \frac{d\epsilon}{2\pi} J_i J_j \text{Im} [\tilde{g}_{m,LR,ij}^{r'}(\epsilon) g_{m,ji}^r(\epsilon)]$$

$$n(\epsilon) \sin \phi,$$

respectively, where $n(\epsilon) = 1/[\exp(\epsilon/k_B T) - 1]$ is the Bose-Einstein distribution function. As seen in Eq. (5), I^c obviously depends on the dynamical spin susceptibility $S_{ij}^m(\epsilon) = -2\text{Im}[g_{m,ij}^r(\epsilon)]$ of the Kitaev QSL, the spectral weight of electron-hole modes $C_{LR,ij}^m(\epsilon) = -2\text{Im}[\tilde{g}_{m,LR,ij}^r(\epsilon)]$ between the two SC leads and the occupation difference between spins and electron-hole modes. Similarly, I^s is weighted by the hybridization spectrum of spins and Cooper pairs $A_{hy,ij}^m(\epsilon) = 2\text{Im}[\tilde{g}_{m,LR,ij}^{r'}(\epsilon) g_{m,ji}^r(\epsilon)]$ and the Bose-Einstein occupation $n(\epsilon)$. In these inelastic scattering processes, the electron-hole modes or Cooper pairs with charge between left and right SC leads transfer energy to the central spin system [25].

Actually, further analysis reveals that both the normal and anomalous Green's functions of the two leads have the same zz , xx and yy components because of the time-reversal symmetry. We have $\tilde{g}_{m,LR,ij}^r(\epsilon) = \tilde{g}_{0,LR,ij}^r(\epsilon)$ and $\tilde{g}_{m,LR,ij}^{r'}(\epsilon) = \tilde{g}_{0,LR,ij}^{r'}(\epsilon)$ for $m = xx, yy$, and zz , respectively. At the same time, the unique feature of QSL leads to that $g_{m,ji}^r(\epsilon)$ is a short-range spin correlation in real space and only the on-site and nearest-neighbour (NN) ones are nonzero, which is explained later in Sec. II C. So the currents have two part contributions from the on-site and NN X, Y, Z bonds. Therefore, we can simplify the tunneling currents I^c and I^s at zero temperature as

$$\begin{aligned}
I^c &= \frac{8e}{\hbar} N J^2 \sum_m \int_0^{eV} \frac{d\epsilon}{2\pi} \left\{ + \sum_{\langle AB \rangle} \text{Im} [\tilde{g}_{0,LR,AA}^r(eV - \epsilon)] \text{Im} [g_{m,AA}^r(\epsilon)] \right. \\
&\quad \left. + \sum_{\langle AB \rangle} \text{Im} [\tilde{g}_{0,LR,BA}^r(eV - \epsilon)] \text{Im} [g_{m,BA}^r(\epsilon)] \right\}, \\
I^s &= \frac{8e}{\hbar} N J^2 \sum_m \int_0^\infty \frac{d\epsilon}{2\pi} \sin \phi \left\{ + \sum_{\langle AB \rangle} \text{Im} [\tilde{g}_{0,LR,AA}^{lr}(\epsilon) g_{m,AA}^r(\epsilon)] \right. \\
&\quad \left. + \sum_{\langle AB \rangle} \text{Im} [\tilde{g}_{0,LR,AB}^{lr}(\epsilon) g_{m,BA}^r(\epsilon)] \right\}. \tag{6}
\end{aligned}$$

Here the indexes of the sublattices, AA and AB, stand for the on-site and NN configurations, and $J_i = J$ for each site i . N is the number of unit cell of honeycomb lattice.

Then, the normal and anomalous two-body Green's functions can be evaluated through the frequency summations over the combinations of left- and right-lead single-body Green's functions, in the 4×4 Nambu representation $(a_{nk\uparrow} a_{n,-k\downarrow}^\dagger a_{nk\downarrow} a_{n,-k\uparrow}^\dagger)$. The details can be seen in Sec. B of *Supplementary Materials* [33]. We thus obtain that

$$\begin{aligned}
\tilde{g}_{0,LR,AA(BA)}^r(\epsilon) &= \frac{s^2}{2} \int \frac{d^2k}{4\pi^2} \int \frac{d^2p}{4\pi^2} e^{i(\mathbf{k}+\mathbf{p}) \cdot \mathbf{R}_{AA(BA)}} \\
&\quad \left\{ \frac{1}{\epsilon - E_{Rp} - E_{Lk} + i0^+} - \frac{1}{\epsilon + E_{Rp} + E_{Lk} + i0^+} \right\} \tag{7a}
\end{aligned}$$

$$\begin{aligned}
\tilde{g}_{0,LR,AA(AB)}^{lr}(\epsilon) &= -\frac{s^2}{2} \int \frac{d^2k}{4\pi^2} \int \frac{d^2p}{4\pi^2} e^{i(\mathbf{k}+\mathbf{p}) \cdot \mathbf{R}_{AA(AB)}} \tag{7b} \\
&\quad \frac{\Delta_L \Delta_R}{E_{Lk} E_{Rp}} \left\{ \frac{1}{\epsilon - E_{Rp} - E_{Lk} + i0^+} - \frac{1}{\epsilon + E_{Rp} + E_{Lk} + i0^+} \right\}
\end{aligned}$$

Here $E_{nk(p)} = \sqrt{\epsilon_{nk(p)}^2 + \Delta_n^2}$, and the parabolic energy dispersions $\epsilon_{Lk} = \hbar^2 k^2 / 2m^* - E_F$, $\epsilon_{Rp} = \hbar^2 p^2 / 2m^* - E_F$. m^* is the effective mass of electron, E_F is the Fermi energy level, and set $\hbar = 1$. s is the area of unit cell of SC-Kitaev layer-SC interface in the SC leads. $R_{AA} = 0$ and $R_{AB} = X, Y, Z$ for the on-site and NN ones, respectively.

Assuming that $k_F = 1/a_s$ and $E_F = 20K$, where k_F and a_s are the Fermi wave vector and lattice constant of two SC leads. Since the exchanged momenta between the SC leads and Kitaev layer are constrained by $0 \leq |\mathbf{q}| \leq 2k_F$, the product $\mathbf{q} \cdot \mathbf{X}(\mathbf{Y}, \mathbf{Z})$ ($\mathbf{q} = \mathbf{k} + \mathbf{p}$) can be taken to zero for simplicity [24, 25] in the Green's functions with the NN contribution. This is suitable for the ‘‘bad metal’’ like Nb or Pb with the small Fermi wave vectors. Hence, in the leads, we have $\tilde{g}_{0,LR,AB(BA)}^r(\epsilon) \approx \tilde{g}_{0,LR,AA(BB)}^r(\epsilon)$ and $\tilde{g}_{0,LR,AB(BA)}^{lr}(\epsilon) \approx \tilde{g}_{0,LR,AA(BB)}^{lr}(\epsilon)$. Then the imaginary part of the normal retarded Green's function of the two SC leads can be further simplified as follows,

$$\begin{aligned}
\text{Im} [\tilde{g}_{0,LR,AA(BA)}^r(\epsilon)] &= -2\pi \rho_L \rho_R \tag{8a} \\
&\quad \left\{ \int_{\Delta_L}^{\epsilon} dE \frac{E}{\sqrt{E^2 - \Delta_L^2}} \frac{(\epsilon - E)}{\sqrt{(\epsilon - E)^2 - \Delta_R^2}}, \epsilon \geq E + \Delta_R \right. \\
&\quad \left. \int_{\Delta_L}^{-\epsilon} dE \frac{E}{\sqrt{E^2 - \Delta_L^2}} \frac{(\epsilon + E)}{\sqrt{(\epsilon + E)^2 - \Delta_R^2}}, \epsilon \leq -E - \Delta_R \right\},
\end{aligned}$$

as well as the imaginary and real parts of the anomalous retarded Green's function

$$\begin{aligned}
\text{Im} [\tilde{g}_{0,LR,AA(AB)}^{lr}(\epsilon)] &= \frac{\pi}{2} \rho_L \rho_R \tag{8b} \\
&\quad \left\{ \int_{\Delta_L}^{\epsilon} dE \frac{\Delta_L}{\sqrt{E^2 - \Delta_L^2}} \frac{\Delta_R}{\sqrt{(\epsilon - E)^2 - \Delta_R^2}}, \epsilon \geq E + \Delta_R \right. \\
&\quad \left. \int_{\Delta_L}^{-\epsilon} dE \frac{\Delta_L}{\sqrt{E^2 - \Delta_L^2}} \frac{-\Delta_R}{\sqrt{(\epsilon + E)^2 - \Delta_R^2}}, \epsilon \leq -E - \Delta_R \right\}, \\
\text{Re} [\tilde{g}_{0,LR,AA(AB)}^{lr}(\epsilon)] &= \int_{-\infty}^{\infty} \frac{d\omega}{2\pi} \frac{(-2) \text{Im} [\tilde{g}_{0,LR,AA(AB)}^{lr}(\omega)]}{\epsilon - \omega}.
\end{aligned}$$

Here we calculate the real part of Green's function by the Kramers-Kronig transformation. The normal density of states (DOS) in the 2D interface $\rho_{L(R)} = m^* a_s^2 / 2\pi \hbar^2$. More details can be seen in Sec. B of *Supplementary Materials* [33].

Therefore, we can obtain the DC single-particle differential conductance dI^c/dV and the derivative of the DC Josephson current I^s with respect to Δ , $dI^s/d\Delta$, as

$$\begin{aligned}
\frac{dI^c}{dV} &= \frac{2e^2}{\hbar} N J^2 \sum_m \int_0^{eV} \frac{d\epsilon}{2\pi} \left\{ \frac{d[C_{LR,AA}^0(eV - \epsilon)]}{dV} S^m(\epsilon) \right\}, \\
\frac{dI^s}{d\Delta} &= \frac{4e}{\hbar} N J^2 \sum_m \int_0^\infty \frac{d\epsilon}{2\pi} \frac{d[A_{hy}^m(\epsilon)]}{d\Delta} \sin \phi. \tag{9}
\end{aligned}$$

Here the total dynamical spin susceptibility, the total hybridization spectrum of spins and Cooper pairs, and the equally weighted spectrum of electron-hole modes are defined as

$$\begin{aligned}
S^m(\epsilon) &= -2 \text{Im} [g_m^r(\epsilon)], \\
A_{hy}^m(\epsilon) &= 2 \text{Im} \{ \tilde{g}_{0,LR,AA}^{lr}(\epsilon) g_m^r(\epsilon) \}, \\
C_{LR,AA}^0(\epsilon) &= -2 \text{Im} [\tilde{g}_{0,LR,AA}^r(\epsilon)], \tag{10}
\end{aligned}$$

respectively, where the total Green's function of spin correlation $g_m^r(\epsilon) = g_{m,AA}^r(\epsilon) + \sum_{\langle AB \rangle} g_{m,BA}^r(\epsilon)$. Once obtaining the Green's functions $\tilde{g}_{0,LR,AA}^r(\epsilon)$, $\tilde{g}_{0,LR,AA}^{lr}(\epsilon)$ and $g_m^r(\epsilon)$, we could get the DC single-particle current and its differential conductance numerically, as well as the zero-voltage Josephson current at zero temperature.

C. Dynamics of the Kitaev model

Next, we need the total Green's function of spin correlation of anisotropic Kitaev QSL, $g_m^r(\epsilon)$, whose imaginary part corresponds to the dynamical spin suscepti-

bility, $S^m(\epsilon)$. We would evaluate the $S^m(\epsilon)$ by employing the few-particle-response method and $g_m^r(\epsilon)$ via the Kramers-Kronig transformation.

The Kitaev model H_{cen} in Eq. (1) can be exactly solved by introducing four Majorana fermions b_i^α ($\alpha = x, y, z$) and c_i per site for the local spins, *i.e.* $\hat{\sigma}_i^\alpha = ic_i b_i^\alpha$. Define the bond operators $\hat{u}_{ij}^\alpha = ib_i^\alpha b_j^\alpha$ on the NN bond $\langle ij \rangle_\Lambda$ ($\Lambda = X, Y, Z$), respectively. Their eigenvalues are $u_{ij}^\alpha = \pm 1$, and they commute with H_{cen} and with each other. So the Kitaev model can be expressed in terms of the different sets of $\{u_{ij}^\alpha\}$ and the Majorana fermions [8, 32],

$$H_{cen} = i \sum_{\Lambda, \langle ij \rangle_\Lambda} K_\Lambda u_{ij}^\alpha c_i c_j, \quad (11)$$

where the product of all bond operators around a plaquette, $W_p = \prod_{i,j \in p} u_{ij}^\alpha \doteq \pm 1$, can define the flux sectors. The eigenstates of this model are Z_2 gauge fluxes threading the plaquettes and Majorana fermions (or spinons) propagating between sites in this Z_2 gauge field [32]. And their wave vectors $|\Phi\rangle$ are the direct product of bond (gauge flux) and Majorana-matter-fermion degrees of freedoms, $|\Phi\rangle = |F\rangle \otimes |M\rangle$. The ground state is within the zero-flux sector with $W_p = 1$ ($u_{ij}^\alpha = 1$) for all plaquettes.

Through the diagonalization of the zero-flux Hamiltonian matrix in the momentum space, the ground-state spinon energy dispersion can be expressed as

$$E_{\mathbf{k}} = 2 |K_X e^{i\mathbf{k}\cdot\mathbf{X}} + K_Y e^{i\mathbf{k}\cdot\mathbf{Y}} + K_Z e^{i\mathbf{k}\cdot\mathbf{Z}}| \quad (12)$$

The ground-state parametric phase diagram is obtained [8], as shown in Fig. 3(a). From Eq. (12), one can find a van Hove singularity at $E_{V1} = 2|K_Z|$ corresponding to the energy contour line PMP' in the first Brillouin region; and another van Hove singularity at $E_{V2} = 2|K_X + K_Y - K_Z|$ when $|K_Z| < 1.5$, or a spinon gap $\Delta_S = 2|K_Z - K_X - K_Y|$ when $1.5 < |K_Z| < 3.0$, associated with the M' point. There is also a energy maximum $E_{max} = 2|K_X + K_Y + K_Z| = 6$ at Γ point. In probing into the dynamical features and evolution of the QSL ground states in the anisotropic Kitaev model, we take the range of the Kitaev couplings K_Z along the line marked by red, blue, and green lines with arrows, labelling the gapped, gapless and another gapless QSL, in this phase diagram. The quantum phases in these three regions display distinct different quantum features [30].

The time-dependent dynamical spin susceptibility of the ground state, $S_{ij}^{\alpha\alpha}(t) = 0.25 \langle \Phi_0 | \hat{\sigma}_i^\alpha(t) \hat{\sigma}_j^\alpha(0) | \Phi_0 \rangle$ ($|\Phi_0\rangle = |F_0\rangle \otimes |M_0\rangle$) [32], can be derived as follows:

$$S_{ij}^{\alpha\alpha}(t) = -0.25i \left\langle M_0 \left| e^{iH_0 t} c_i e^{-i(H_0 + V_{(ij)\Lambda})t} c_j \right| M_0 \right\rangle \\ (i\delta_{ij} + \hat{u}_{ij}^\alpha \delta_{(ij),\Lambda}), \quad (13)$$

where $V_{(ij)\Lambda} = -2iK_\Lambda c_i c_j$, $i \in A, j \in B$, and $\alpha = x, y, z$ corresponds to $\Lambda = X, Y, Z$ one-to-one. We can find that only the on-site (δ_{ij}) and NN ($\delta_{(ij),\Lambda}$) ones of the dynamical spin correlation are non-zero, and $S_{ij}^{\alpha\alpha}$ only has the $\alpha = z(x, y)$ component in the NN $X(Y, Z)$ -bond.

$S_{ij}^{\alpha\alpha}$ has the *Lehmann* representation by inserting the identity $\mathbf{1} = \sum_\lambda |\lambda\rangle \langle \lambda|$ of the two-flux sector with a flipping bond $u_{ij}^\alpha = -1$. The main contributions are from the zero-, one- and two-particle of $|\lambda\rangle$, which occupy the 98% of the total [32]. We thus can obtain the dynamical spectrums in the frequency ω -space as

$$S_{AA}^{\alpha\alpha}(\omega) = \frac{\pi}{2} \sum_\lambda \langle M_0 | c_A |\lambda\rangle \langle \lambda | c_A | M_0 \rangle \delta[\omega - (E_\lambda^F - E_0)], \\ S_{BA}^{\alpha\alpha}(\omega) = \frac{\pi}{2} i \sum_\lambda \langle M_0 | c_B |\lambda\rangle \langle \lambda | c_A | M_0 \rangle \delta[\omega - (E_\lambda^F - E_0)]. \quad (14)$$

Here E_0 is the ground-state energy of the zero-flux sector, and E_λ^F is the energy eigenvalue of the [32]state $|\lambda\rangle$ of two-flux sector, while the lowest-energy is E_0^F with the state $|M_F^{z(x,y)}\rangle$. $|\lambda\rangle$ and E_λ^F are obtained through the diagonalization of the two-flux Hamiltonian matrix in the real space. Further we can calculate the overlaps $\langle M_0 | M_F^{z(x,y)} \rangle^2$ and ‘‘vison’’ gap $\Delta_F^{z(x,y)} = E_0^F - E_0$ due to the gauge-flux excitation, as shown in Fig. 3(b)(c), consistent with Knolle’s results [32].

From the dynamical phase diagrams in Fig. 3(b)(c), we can see that the lowest-energy states of the zero-flux sector H_0 and two-flux sector $H_0 + V_{z(x,y)}$, $|M_0\rangle$ and $|M_F^{z(x,y)}\rangle$ conserve the parity owing to the spatial inversion symmetry. Along the line in Fig. 3(a), $|M_0\rangle$ and $|M_F^z\rangle$ have the same parity when $1.24 < |K_Z| < 3.0$ and the opposite parity when $0 < |K_Z| < 1.24$; $|M_0\rangle$ and $|M_F^{x(y)}\rangle$ have the same parity all the way. In the case with the same parity, $|\lambda\rangle$ must contain the odd number of excitations, mainly the single-particle contribution. This dynamical spin susceptibilities could be evaluated by Eq.(12). In the opposite case, $|\lambda\rangle$ must contain the even number of excitations, mainly the zero- and two-particle contributions. Actually the *Lehmann* representation is modified by inserting the identity $\mathbf{1} = \sum_\lambda c_{A(B)} |\lambda\rangle \langle \lambda | c_{A(B)}$ of two-flux sector $H_0 + V_x + V_y$ with two flipping bonds $u_{ij}^x, u_{ij}^y = -1$. Its lowest-energy state $|M_F^{x,y}\rangle$ have the same parity with $|M_0\rangle$ [32], as shown in Fig. 3(b). We also plot the lowest-energy state $|M_F^{y,z}\rangle$ for $H_0 + V_y + V_z$ shown in Fig. 3(c). It has the opposite parity with $|M_0\rangle$ all the way. Therefore, we can explicitly express Eq. (11) for the zero- and two-particle contributions,

$$S_{AA}^{\alpha\alpha}(\omega) = \frac{\pi}{2} \sum_\lambda \langle M_0 | \lambda \rangle \langle \lambda | M_0 \rangle \delta[\omega - (E_\lambda^F - E_0)], \quad (15)$$

$$S_{BA}^{\alpha\alpha}(\omega) = \frac{\pi}{2} i \sum_\lambda \langle M_0 | c_B c_A |\lambda\rangle \langle \lambda | M_0 \rangle \delta[\omega - (E_\lambda^F - E_0)].$$

Then the dynamical spin correlation $S^m(\epsilon) = S_{AA}^m(\epsilon) + S_{BA}^m(\epsilon)$ ($m = \alpha\alpha, \alpha = x, y, z$). More details are shown in Sec. C of *Supplementary Materials* [33]. Hence, combining the dynamical and parametric phase diagrams, we choose four representative points $K_Z = 1.8, 1.4, 1.0$ and 0.6 , respectively, among the phase transition points about the parity relationship and spinon gap, $K_Z = 1.24$ and 1.5 .

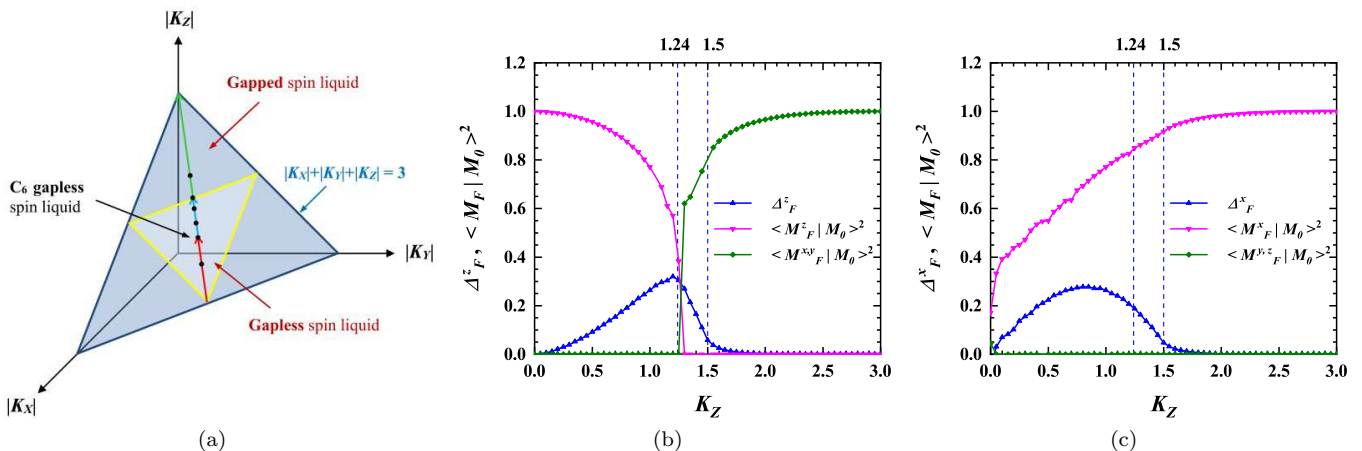


FIG. 3. (Color online) (a) The variation range of Kitaev coupling strengths in the parametric phase diagram of the Kitaev model with the conditions $K_X = K_Y$ and $K_X + K_Y + K_Z = 3.0$, marked by red, blue and green arrows. Six points are marked with black dots, $K_Z = 1.8, 1.5, 1.4, 1.24, 1.0$, and 0.6 . Kitaev coupling K_Z dependences of (b) the overlaps $\langle M_F^z | M_0 \rangle^2$, $\langle M_F^{x,y} | M_0 \rangle^2$ and vison gap Δ_F^z , and (c) the overlaps $\langle M_F^x | M_0 \rangle^2$, $\langle M_F^{y,z} | M_0 \rangle^2$ and vison gap Δ_F^x in the variation range of (a).

Substituting the Eq. (8),(14) and (15) into Eq. (6), (9) and (10), we can obtain the tunneling current $I^{c,s}$ and differential conductances dI^c/dV and $dI^s/d\Delta$. Throughout this *paper* the SC order parameters $\tilde{\Delta}_L$ and $\tilde{\Delta}_R$ in the left and right leads have the same modulus $\Delta_L = \Delta_R = \Delta$, but different phase $\phi_{L(R)}$. In this paper, all of the energies are measured in terms of the Kitaev coupling K , which can be taken as $K = 1$.

III. RESULTS AND DISCUSSION

A. Dynamical spin correlations of the anisotropic Kitaev model

At first, we plot the dynamical spin susceptibilities of the anisotropic Kitaev model, including the components $S^{\alpha\alpha}(E)$ ($\alpha = x, y, z$) and their total S^{tot} , as functions of energy E [24–26, 31, 32], as shown in Fig. 4(a)-(d). Here $S^{xx} = S^{yy}$ because $K_X = K_Y$. From this, we can see that the anisotropic components of dynamical spin susceptibilities, S^{zz} and $S^{xx(yy)}$, and their total S^{tot} reveal remarkable different features in these four quantum phases.

When $K_Z = 1.8$ with a gapped QSL, the parities between $|M_F^z\rangle$ and $|M_0\rangle$ are opposite. As shown in Fig. 4(a), in $S^{xx(yy)}$, we can see the total QSL gap $\Delta_t \approx 1.2$. It actually contains the spinon gap $\Delta_S = 2|K_Z - K_X - K_Y| = 1.2$ and vison gap $\Delta_F^x \approx 0.0$. There is a dip at $E \approx 3.6$ owing to the van Hove singularity of spinon spectrum at $2K_Z$ and an energy shift of Δ_F^x . And an upper edge emerges at about 6.0 which equals $\Delta_F^x + 2|K_X + K_Y + K_Z|$. So these three feature points in $S^{xx(yy)}$ correspond to the ones of spinon dispersion at E_V (Δ_S or E_{V1} , E_{V2} and E_{max}) one-to-one, and move towards $\Delta_F^{x(y)} + E_V$. There is a new peak at about 2.5

caused by the interacting vison and spinon. However, in S^{zz} , we can observe the total gap $\Delta_t' \approx 2.4$, which stems from the $\Delta_F^z \approx 0.0$ and the new spinon gap $\Delta_S' = 2\Delta_S$. A peak appears at $E \approx 7.2$ resulted from the van Hove singularity, and the upper edge emerges at $E \approx 12.0$. The three feature points at $\Delta_F^z + 2E_V$ in S^{zz} are from the virtual transitions to the eigenstates of two-flux sector with two flipping bonds. Moreover, we can see a distinct sharp peak at Δ_F^z , stemmed from the virtual transitions to the lowest-energy state, $|M_F^{x,y}\rangle$. There is also a new peak around 5.0 due to the interaction of vison and spinon. Note that $S^{xx(yy)}$ is an order of magnitude bigger than S^{zz} . As for the sum of S^{zz} , S^{xx} and S^{yy} , S^{tot} can exhibit the complete information of vison, spinon and their interaction, except some feature points because of the resolution of S^{zz} .

When $K_Z = 1.4$ shown in Fig. 4(b), the ground-state is gapless QSL and $|M_F^z\rangle$ and $|M_0\rangle$ have the opposite parity. Hence, the three feature points are displayed on $S^{xx(yy)}$ and S^{zz} in the similar way as $K_Z = 1.8$, except the van Hove singularity instead of the spinon gap. In S^{xx} , we can observe two dips at $E \approx 0.5$ and 2.9 corresponding to the van Hove singularities, and an upper edge at about 6.1 with $\Delta_F^x \approx 0.11$. These three feature points emerge at $\Delta_F^{x(y)} + E_V$. There are two new interaction peaks at about 0.4 and 1.5. In S^{zz} , there is a dip and an inflection point associated with the van Hove singularities at $E \approx 1.0$ and 5.8 , and a boundary at about 12.2 with $\Delta_F^z \approx 0.17$. So these feature points are shown at $\Delta_F^z + 2E_V$. A remarkable sharp peak appears at Δ_F^z , and a new interaction peak emerges at about 0.8. Since S^{zz} has the same order in magnitude to $S^{xx,yy}$, the total one S^{tot} could reveal the full dynamical features of Kitaev QSL well.

When $K_Z = 1.0$ and 0.6 , as shown in Fig. 4(c)(d), $|M_F^{z(x,y)}\rangle$ and $|M_0\rangle$ have the same parity. At $K_Z = 1.0$,

the ground-state of the isotropic Kitaev model is a C_6 gapless QSL, and $S^{xx(yy)}$ and S^{zz} components are equal, $\Delta_F^{x(y)} = \Delta_F^z \approx 0.26$. From S^{zz} we can find that there is only one dip related to the two-in-one van Hove singularity at $E \approx 2.26$, and a upper edge at about 6.26. There is also a new interaction peak at about 0.5. At $K_Z = 0.6$, two dips resulted from the van Hove singularities, a upper edge and a new sharp peak are shown at $E \approx 1.45, 3.85, 6.25$ and 0.3 in $S^{xx(yy)}$ with $\Delta_F^{x(y)} \approx 0.25$. There is a dip and a inflection point, a upper boundary and a new peak at $E \approx 1.32, 3.72, 6.12$ and 0.8 in S^{zz} with $\Delta_F^z \approx 0.12$. Therefore, the feature points emerge at $\Delta_F^{x(y)} + E_V$ and $\Delta_F^z + E_V$ in $S^{xx(yy)}$ and S^{zz} , respectively, because of the virtual transitions to the eigenstates of two-flux sector with only a flipping $X(Y)$ - or Z -bond. The total spin correlations S^{tot} also have the entire characters of Kitaev QSL when $K_Z = 1.0$ and 0.6 .

In a word, the dynamical spin susceptibility components S^{zz} and $S^{xx}(=S^{yy})$ reveal different vison gaps Δ_F^z and $\Delta_F^{x(y)}$, respectively. Every component can only reveal the partial features of the Majorana fermion (spinon) dispersions influenced by the gauge fluxes, including the two van Hove singularities (or a spinon gap and a van Hove singularity) and the energy upper edge, and in different ways. Therefore, the total S^{tot} can exhibit the complete information of Kitaev QSL well. There are some new peaks between these feature points, which stem from the interaction between the vison and spinon excitations.

B. DC Josephson current with zero voltage

In the absence of the bias voltage, only the DC *Josephson* current with the tunneling of the Cooper pairs is presented in the SC-Kitaev QSL-SC junction. The SC gap Δ dependences of the derivative of the DC *Josephson* current I^s with respect to Δ , $G_{tot} = dI^s/d\Delta$, and its components $G_{z(x,y)}$ ($G_x = G_y$) have been described in Fig. 5(a)-(d) for different Kitaev couplings $K_Z = 1.8, 1.4, 1.0$ and 0.6 , respectively. Here the phase difference $\phi = 3\pi/2$ and we define the dimensionless constant $g_0 = 4\pi\rho_L\rho_R J^2$.

As seen in Fig. 5(a)-(d), when $K_Z = 1.8$, we can see a peak at $\Delta \approx 0.6$, and an inflection point at about 1.25. The former corresponds to the total QSL gap $\Delta_t \approx 1.2$, which originates from the resonant tunneling when $2\Delta = \Delta_t$, while the latter stems from the interaction between the vison and spinon excitations near $2\Delta \approx 2.5$. Similarly, at $K_Z = 1.4$, a distinct peak, corresponding to the total QSL gap, emerges around $2\Delta \approx 0.17$. Another peak at about 0.9 stemming from the response to the interaction peak appears near $2\Delta \approx 1.8$. When $K_Z = 1.0$ and 0.6 , we can only observe the peaks at about 0.25 and 0.4, which are due to the response to the interaction peaks around $2\Delta \approx 0.5$ and 0.8 , respectively. Thus, $dI^s/d\Delta$ curves mainly provide the information about the interaction of gauge fluxes and Majorana fermion mode, as well as the total QSL gap. These peaks in $dI^s/d\Delta$

could be seen from the dynamical spin susceptibilities in Fig. 4, however, only partially provide full information of the Kitaev QSLs.

To understand this reason, we plot the energy E dependences of the total dynamical hybridization spectral functions between local spins of the Kitaev layer and Cooper pairs of the two SC leads, $A_{hy} = \sum_{\alpha} A_{hy}^{\alpha\alpha}$ ($\alpha = x, y, z$), in Fig. 6(a)-(d). The SC gaps are set as $\Delta=1, 3$, and 5 , respectively. From Fig. 6 we can see the whole dynamical spin correlation characters clearly and $A_{hy} > 0$ before $E = 2\Delta$. When $E > 2\Delta$, these spin correlation features appear with a reversal sign, *i.e.* $A_{hy} < 0$ in the same magnitude. Thus, the DC *Josephson* current at zero bias, as the frequency integration of the hybridization spectrum, is partially cancelled; hence, it only keeps partial information of Kitaev QSL. This arises from the fact that in the inelastic tunneling, the quasi-electrons and quasi-holes of the SC Cooper pairs contribute the positive and negative parts of the A_{hy} , respectively. Therefore, the total response to the dynamical spin correlation spectrum is cancelled out due to the spin-singlet Cooper pairs.

C. DC conductance of the normal single-particle tunneling

Further, in the presence of a DC bias voltage in the SC-Kitaev QSL-SC junction, one could reveal more characters of the Kitaev QSL. The bias potential eV dependences of the DC single-particle differential conductance $G_{tot}=dI^c/dV$, as well as its $zz(xx,yy)$ components $G_{z(x,y)}$, have been described in Fig. 7(a)-(d) for different Kitaev couplings $K_Z = 1.8, 1.4, 1.0$ and 0.6 , respectively. Here we define the conductance constant $G_0 = g_0 e^2/h$, and $G_{tot} = G_x + G_y + G_z$ with $G_x = G_y$.

From Fig. 7(a)-(d), the single-particle DC differential conductance spectrums of the SC junction, G_{tot} and $G_{z(x,y)}$, show the distinct different characters in the four quantum phases. To clearly see the dynamical behaviors of G_{tot} in present anisotropic Kitaev layer, we first describe the bias voltage dependence of $G_{z(x,y)}$. When $K_Z = 1.8$, as seen in Fig. 7(a), contrast with the dynamical spin susceptibility in Fig. 4(a), the threshold of the conductance $G_{x(y)}$ is modulated up to about 3.2 , *i.e.* $\Delta_t + 2\Delta$. This arises from the fact that the electrons at the bottom of the SC gap in the right lead need a high enough bias potential $eV = \Delta + \Delta + \Delta_t$ to overcome the right and left SC gaps and total QSL gap of the central layer along the X -(Y -) bond, and finally reach the empty state on the top of the SC gap in the left lead. When $eV > 2\Delta + \Delta_t$, with the open of the channel of the Majorana bond state, the conductance $G_{x(y)}$ starts to rise rapidly and goes up to a sharp peak at about 4.5. This peak corresponds to the interaction peak of the dynamical spin correlation around 2.5 shown in Fig. 4(a), and results from the dynamical creation of the Majorana fermions (or spinon) interacting with the NN two gauge fluxes in the virtual transition. Soon afterwards, a re-

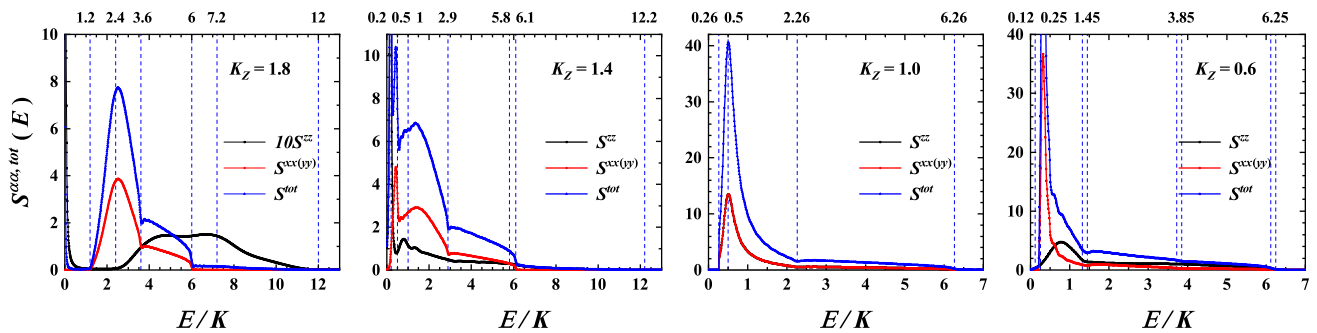


FIG. 4. (Color online) Energy E dependences of the dynamical spin susceptibilities of the anisotropic Kitaev QSL, including the total S^{tot} and its three components $S^{\alpha\alpha}(q=0, E)$ ($\alpha = x, y, z$) for different Kitaev coupling $K_Z = 1.8$ (a), 1.4 (b), 1.0 (c) and 0.6 (d), respectively, in units of the energy K . Here $S^{xx} = S^{yy}$

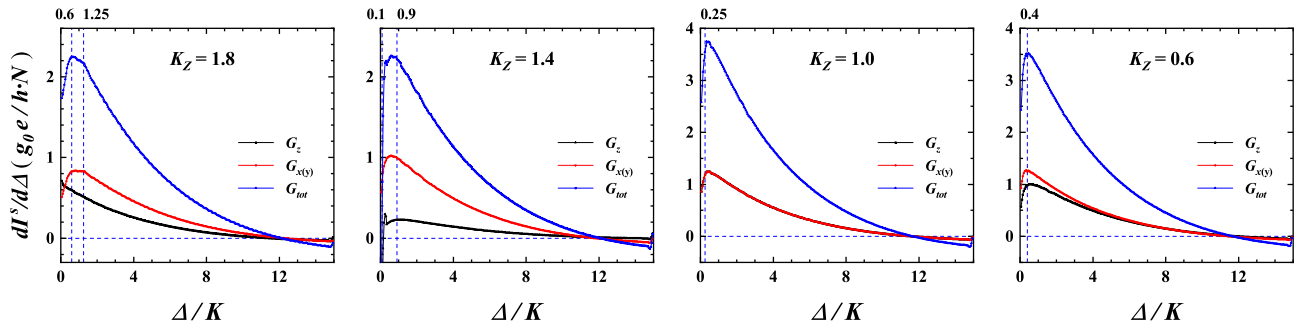


FIG. 5. (Color online) Derivative of the DC *Josephson* tunneling current I^s with respect to the SC gap, $dI^s/d\Delta$, including the components $G_{z(x,y)}$ ($G_x = G_y$) and the total G_{tot} , as functions of the SC gap Δ for different Kitaev coupling $K_Z = 1.8$ (a), 1.4 (b), 1.0 (c) and 0.6 (d), respectively. Here $\phi = 3\pi/2$

markable dip have been observed at about 5.6, which is associated with the dip of dynamical spectrum around 3.6 and due to the van Hove singularities of the DOS of the Majorana dispersive band. Finally, the single-particle conductance approaches to a constant after the upper edge at about 8 due to the one of Majorana dispersive band around 6. Hence, the features of the single-particle DC differential conductance spectrums $G_{x(y)}$ in Fig. 7(a) correspond to those of the dynamical spin susceptibility one-to-one in Fig. 4(a).

Meanwhile, we can see a remarkable sharp peak at $eV \approx 2$ in G_z related to the one in the dynamical spectrum near $\Delta_z^F \approx 0.0$, which originates from the δ -function contribution of the virtual transition between the ground state $|M_0\rangle$ and the excited state $|M_F^{x,y}\rangle$. When $eV > \Delta_z^F$, no obvious characters in G_z is observed since S^{zz} is an order of magnitude smaller than $S^{xx(yy)}$. Summing the three components gives rise to the total conductance G_{tot} , which contains the complete characters of the spinon spectrums, vison excitation and their interaction of Kitaev QSL. Thus, compared to the normal-metal junction situation[24, 25], the present differential conductance spectrums G_{tot} have a more intuitive and sensitive response to the characters of dynamical spin correlation components of Kitaev QSL, S^{tot} .

When $K_Z = 1.4, 1.0$ and 0.6, similar to $K_Z = 1.8$, the single-particle DC differential conductance spectrums $G_{z(x,y)}$ can reflect the features of dynamical spin susceptibility components $S^{zz(x,y)}$ well, except some feature points due to the resolution in numerical integration. Fortunately, in the present situations with $K_Z = 1.4, 1.0$ and 0.6, the z-component of dynamical spin correlations S^{zz} are the same order in magnitude to $S^{xx,yy}$, so G_z can resolve the complete features of S^{zz} . Hence, from the single-particle tunneling spectrums, we could get insight into the features of the dynamical spin susceptibilities of Kitaev QSL.

IV. CONCLUSION

In our present theory, we point out two possible improvements to the present results. On the one hand, with the condition of $\mathbf{q} \cdot \mathbf{X}(\mathbf{Y}, \mathbf{Z}) \approx 0$, we obtain the features of the total dynamical spin susceptibility S^{tot} . When $\mathbf{q} \cdot \mathbf{X}(\mathbf{Y}, \mathbf{Z}) \neq 0$, the individual contribution of each component of the NN spin correlation $S_{BA}^{\alpha\alpha}$ to the tunneling currents would be slightly different from the result above. Our further study reveals that in this situation the correction to Eq. (8) only quantitatively alters the tunneling

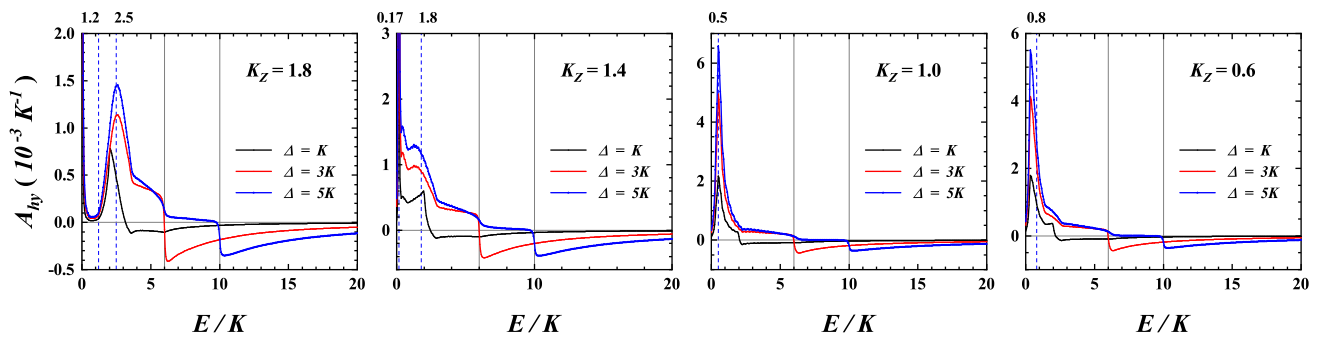


FIG. 6. (Color online) Energy E dependences of the total hybridization spectral functions between spins of the central Kitaev QSL layer and Cooper pairs of the two SC leads, A_{hy} , with $\Delta=1, 3$ and 5 for different Kitaev coupling $K_Z = 1.8$ (a), 1.4 (b), 1.0 (c) and 0.6 (d), respectively.

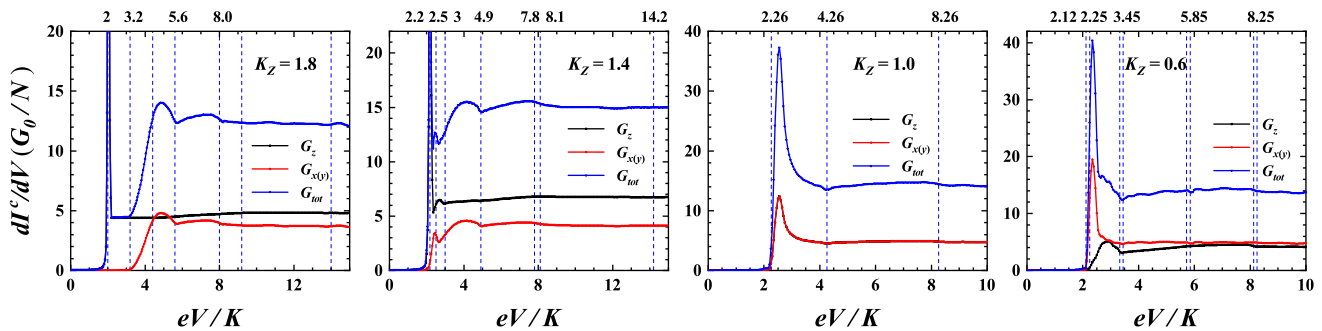


FIG. 7. (Color online) DC differential conductances of the single-particle tunneling dI^c/dV , including the components $G_{z(x,y)}$ ($G_x = G_y$) and the total G_{tot} , as functions of the bias potential eV for different Kitaev coupling $K_Z = 1.8$ (a), 1.4 (b), 1.0 (c) and 0.6 (d), respectively.

current, nevertheless, it is qualitatively consistent with the above conclusion. On the other hand, although the zero-voltage *Josephson* current fails to measure the full information of the Kitaev QSL in the elastic scattering process, we expect that the AC *Josephson* currents with DC bias voltage can reveal more features of dynamical spin correlation, which goes beyond the scope of this paper.

As a summary, in investigating the electron tunneling transport and its spectroscopic features in an SC-anisotropic Kitaev QSL-SC *Josephson* junction with the weak link, we assume that the inelastic scattering tunneling of the single particle and Cooper pair is realized by the $s - d$ exchange interaction. As expected, the DC differential conductance dI^c/dV of the normal single-particle tunneling succeeds in exhibiting the dynamical spin susceptibility characters of the anisotropic Kitaev QSL, including the unique spin gaps even in gapless QSL, the sharp or broad peaks, the small dips and the upper edge of the itinerant Majorana fermion dynamics, except an energy shift of two-SC-lead gap 2Δ . The different

topological quantum phases of anisotropic Kitaev QSL can be distinguished by the tunneling spectral features well. Unusually, the zero-voltage DC *Josephson* currents I^s only have some residual information of Kitaev QSL, which stems from the spin singlet of Cooper pairs. Our results may pave a new way to measure the Majorana-fermion dynamical correlation features of the anisotropic Kitaev and other spin liquid materials. We expect that our theoretical results could be confirmed by future experiments and be applied in the SC junction devices.

ACKNOWLEDGMENTS

L. J. thanks the supports from the NSFC of China under Grant Nos.11774350 and 11474287, H.Q. acknowledges financial support from NSAF U1930402 and NSFC 11734002. Numerical calculations were performed at the Center for Computational Science of CASHIPS and Tianhe II of CSRC.

[1] L. Balents, Spin liquids in frustrated magnets, Nature (London) **464**, 199 (2010).

[2] Z. Y. Meng, T. C. Lang, S. Wessel, F. F. Assaad, and

- A. Muramatsu, Quantum spin liquid emerging in two-dimensional correlated dirac fermions, *Nature* **464**, 847 (2010).
- [3] P. W. Anderson, Resonating valence bonds: A new kind of insulator?, *Mater. Res. Bull.* **8**, 153 (1973).
- [4] P. Fazès and P. W. Anderson, On the ground state properties of the anisotropic triangular antiferromagnet, *Philos. Mag.* **30**, 423 (1974).
- [5] F. Mezzacapo and M. Boninsegni, Ground-state phase diagram of the quantum j1-j2 model on the honeycomb lattice, *Phys. Rev. B* **85**, 060402(R) (2012).
- [6] X.-L. Yu, D.-Y. Liu, P. Li, and L.-J. Zou, Ground-state and finite-temperature properties of spin liquid phase in the j1-j2 honeycomb model, *Physica E* **59**, 41 (2014).
- [7] G. Jackeli and G. Khaliullin, Mott insulators in the strong spin-orbit coupling limit: From heisenberg to a quantum compass and kitaev models, *Phys. Rev. Lett.* **102**, 017205 (2009).
- [8] A. Kitaev, Anyons in an exactly solved model and beyond, *Ann. Phys. (N. Y.)* **321**, 2 (2006).
- [9] A. Kitaev, Fault-tolerant quantum computation by anyons, *Ann. Phys. (N. Y.)* **303**, 2 (2003).
- [10] N. Read and B. Chakraborty, Statistics of the excitations of the resonating-valence-bond state, *Phys. Rev. B* **40**, 7133 (1989).
- [11] S. S. Hegde, G. Yue, Y. X. Wang, E. Huemiller, D. J. Van Harlingen, and S. Vishveshwara, A topological josephson junction platform for creating, manipulating, and braiding majorana bound states, *Ann. Phys. (N. Y.)* **423**, 168326 (2020).
- [12] S. V. Bakurskiy, A. A. Golubov, and M. Y. Kupriyanov, *Fundamentals and Frontiers of the Josephson Effect* (Springer-Verlag, Napoli, Italy, 2019).
- [13] T. Xiang, *D-Wave Superconductivity* (Science and Education Press, Beijing, China, 2007).
- [14] A. W. Kleinsasser, R. E. Miller, W. H. Mallison, and G. B. Arnold, Observation of multiple andreev reflections in superconducting tunnel junctions, *Phys. Rev. Lett.* **72**, 1738 (1994).
- [15] A. F. Morpurgo, B. J. van Wees, T. M. Klapwijk, and G. Borghs, Energy spectroscopy of andreev levels between two superconductors, *Phys. Rev. Lett.* **79**, 4010 (1997).
- [16] Q.-F. Sun, B.-G. Wang, J. Wang, and T.-H. Lin, Electron transport through a mesoscopic hybrid multiterminal resonant-tunneling system, *Phys. Rev. B* **61**, 4754 (2000).
- [17] Y. Zhu, Q.-F. Sun, and T.-H. Lin, Andreev reflection through a quantum dot coupled with two ferromagnets and a superconductor, *Phys. Rev. B* **65**, 024516 (2001).
- [18] Q.-F. Sun, H. Guo, and J. Wang, Hamiltonian approach to the ac josephson effect in superconducting-normal hybrid systems, *Phys. Rev. B* **65**, 075315 (2002).
- [19] E. A. Demler, G. B. Arnold, and M. R. Beasley, Superconducting proximity effects in magnetic metals, *Phys. Rev. B* **55**, 15174 (1997).
- [20] V. V. Ryazanov, V. A. Oboznov, A. Y. Rusanov, A. V. Veretennikov, A. A. Golubov, and J. Aarts, Coupling of two superconductors through a ferromagnet: Evidence for a π junction, *Phys. Rev. Lett.* **86**, 2427 (2001).
- [21] E. C. Gingrich, B. M. Niedzielski, J. A. Glick, Y. X. Wang, D. L. Miller, R. Loloee, W. P. Pratt Jr, and N. O. Birge, Controllable $0-\pi$ josephson junctions containing a ferromagnetic spin valve, *Nature Phys.* **12**, 564 (2016).
- [22] L. P. Gor'kov and V. Z. Kresin, Josephson junction with an antiferromagnetic barrier, *Physica C* **367**, 103 (2002).
- [23] L. Bulaevskii, R. Eneias, and A. Ferraz, Superconductor-antiferromagnet-superconductor π josephson junction based on an antiferromagnetic barrier, *Phys. Rev. B* **95**, 104513 (2017).
- [24] M. Carrega, I. J. Vera-Marun, and A. Principi, Tunneling spectroscopy as a probe of fractionalization in two-dimensional magnetic heterostructures, *Phys. Rev. B* **102**, 085412 (2020).
- [25] E. J. König, M. T. Randeria, and B. Jäck, Tunneling spectroscopy of quantum spin liquids, *Phys. Rev. Lett.* **125**, 267206 (2020).
- [26] J. Feldmeier, W. Natori, M. Knap, and J. Knolle, Local probes for charge-neutral edge states in two-dimensional quantum magnets, *Phys. Rev. B* **102**, 134423 (2020).
- [27] Y. Yamaji, T. Suzuki, T. Yamada, S.-I. Suga, N. Kawashima, and M. Imada, Clues and criteria for designing a kitaev spin liquid revealed by thermal and spin excitations of the honeycomb iridate Na_2IrO_3 , *Phys. Rev. B* **93**, 174425 (2016).
- [28] S. K. Choi, R. Coldea, A. N. Kolmogorov, T. Lancaster, I. I. Mazin, S. J. Blundell, P. G. Radaelli, Y. Singh, P. Gegenwart, K. R. Choi, S.-W. Cheong, P. J. Baker, C. Stock, and J. Taylor, Spin waves and revised crystal structure of honeycomb iridate Na_2IrO_3 , *Phys. Rev. Lett.* **108**, 127204 (2012).
- [29] A. Banerjee, C. A. Bridges, J.-Q. Yan, A. A. Acze, L. Li, M. B. Stone, G. E. Granroth, M. D. Lumsden, Y. Yiu, J. Knolle, S. Bhattacharjee, D. L. Kovrizhin, D. A. T. R. Moessner, D. G. Mandrus, and S. E. Nagler, Proximate kitaev quantum spin liquid behaviour in a honeycomb magnet, *Nature Mater.* **15**, 733 (2016).
- [30] S.-Q. Jia, Y.-M. Quan, H.-Q. Lin, and L.-J. Zou, Topological quantum phase transitions of anisotropic afm kitaev model driven by magnetic field, arXiv:2104.12935 (2021).
- [31] J. Knolle, D. L. Kovrizhin, J. T. Chalker, and R. Moessner, Dynamics of a two-dimensional quantum spin liquid: Signatures of emergent majorana fermions and fluxes, *Phys. Rev. Lett.* **112**, 207203 (2014).
- [32] J. Knolle, *Dynamics of a Quantum Spin Liquid* (Springer-Verlag, Heidelberg, Berlin, Germany, 2016).
- [33] See supplementary materials to this publication.